



## Bone incineration: An experimental study on mineral structure, colour and crystalline state

M. Greiner<sup>a,\*</sup>, A. Rodríguez-Navarro<sup>b</sup>, M.F. Heinig<sup>a</sup>, K. Mayer<sup>c</sup>, B. Kocsis<sup>a</sup>, A. Göhring<sup>c</sup>, A. Toncalo<sup>c</sup>, G. Grupe<sup>c</sup>, W.W. Schmahl<sup>a</sup>

<sup>a</sup> Department für Geo- und Umweltwissenschaften, Ludwig-Maximilians-Universität, 80333 Munich, Germany

<sup>b</sup> Departamento Mineralogía y Petrología, Facultad de Ciencias, Universidad de Granada, Campus Fuentenueva, 18071 Granada, Spain

<sup>c</sup> Fakultät für Biologie, Anthropologie und Humangenomik, Ludwig-Maximilians-Universität, 82152, Planegg-Martinsried, Germany



### ARTICLE INFO

**Keywords:**

Bioapatite  
Carbonated apatite  
Rietveld method  
Calcination  
Forensic science  
Crystallinity index  
Bioarchaeology

### ABSTRACT

Unheated and heat-treated bovine bone material with differing heating times and heat-treated in increments from 100 °C to 1000 °C were analysed to study the crystallographic change of fresh biological bone mineral occurring during incineration. We combine several complementary analytical methods applied to the same unheated and heat treated material to ensure data consistency in order to establish a comprehensive study on heat-induced changes in bone. We applied quantitative powder X-ray diffraction, Fourier Transform Infrared Spectroscopy (FTIR), and Infrared-coupled Thermogravimetric Analysis (TGA-FTIR), and we correlated the analytical results with empirical indicators such as crystallinity indices (CI and IRSF) and bone colour changes after burning. At temperatures from 700 °C onwards after 30 min of heating, a considerable recrystallization reaction from bioapatite to hydroxyapatite occurred. FTIR revealed that there are no or only minor amounts of hydroxyl-ions in original bone mineral which in consequence should be referred to “carbonate-hydro-apatite” rather than hydroxyapatite. Thermal treatment induced a pronounced increase of crystallite size and an increase of hydroxyl groups in the apatite lattice accompanied by a depletion of water and reduction of carbonate contents during incineration. Thus, the heat treatment at temperatures ≥700 °C leads to the recrystallization of bioapatite to hydroxyapatite. Above 800 °C buchwaldite is formed from the Na component within the bone mineral. Moreover, we found that the transformation reaction involving crystallite growth mainly sets in after organic matrix compounds and their residues have been combusted and the apatite grains get into direct contact. The information in this work, obtained by a combination of analytical methods which are typically applied and approved to determine bone cremation temperatures, can help to better understand changes in complex biomaterials during heating. In particular, the knowledge from this study can be applied to assess the cremation conditions of archaeological bone finds. As changes in the bone mineral state are not only dependent on temperature but also on time, care must be taken to deduce a defined temperature which cremated bone finds were exposed to.

### 1. Introduction

From the late Bronze Age to Imperial Roman Times, the preferred manner of human burial in some parts of Europe was to cremate the bodies (Grupe et al., 2015). Structural and chemical analyses revealed that archaeological cremated bone remains from the Bronze Age (Urnfield Culture) in southern Bavaria were exposed to temperatures estimated from 700 °C to 1000 °C (Grupe et al., 2017). In archaeology, a first estimation of the heating temperature is usually based on the colour of the bone finds. Burn colour codes defined for example by Wahl (1982) or Stiner et al. (1995) are used to categorise heat exposure

based on bone macroscopic appearance and colour. Since the colour of burnt bones is not only a consequence of temperature and the duration of heat-exposure (e.g. Herrmann, 1977; Shipman et al., 1984; Von Endt and Ortner, 1984; Nicholson, 1993; Sillen and Hoering, 1993; Bennett, 1999; Thompson, 2005; Thompson et al., 2016) but also dependent on the availability of oxygen (Walker et al., 2008) or influenced by inclusions of exogenous elements within the bone mineral such as copper (Dunlop, 1978), it takes additional analytical methods to define the temperature which bone finds were exposed to.

Over the last years there's been various research on quantitative analytical methods such as X-ray diffraction (XRD) and Fourier

\* Corresponding author.

E-mail address: [martina.greiner@lrz.uni-muenchen.de](mailto:martina.greiner@lrz.uni-muenchen.de) (M. Greiner).

Transform Infrared Spectroscopy (FTIR, KBr-method) analysis to understand heat-induced changes in bone in forensic, archaeological and anthropological contexts (e.g. Shipman et al., 1984; Rogers and Daniels, 2002; Hiller et al., 2003; Enzo et al., 2007; Thompson and Chudek, 2007; Munro et al., 2007, 2008; Lebon et al., 2008; Piga et al., 2008, 2009; Thompson et al., 2009; Snoek et al., 2014; Mamede et al., 2018; Piga et al., 2018). XRD and full pattern analysis like the Rietveld method (Rietveld, 1969) are suitable methods for the calibration of the temperature bones were exposed to (Holden et al., 1995; Person et al., 1996; Harbeck et al., 2011; Galeano and García-Lorenzo, 2014). FTIR provides complementary detailed information about the chemical composition and structure of the main components of the bone material and their changes in consequence of thermal treatment (e.g. Weiner et al., 1993; Thompson et al., 2009). The thermal decomposition behaviour of bone has been thoroughly studied by e.g. Bonucci and Graziani (1975) and Ellingham et al. (2015) by Thermogravimetric Analysis (TGA).

However, some incommensurabilities remain and a direct comparison of the results reported by the mentioned authors is not feasible as different starting materials were investigated. In order to gain a deeper understanding about bone alteration by cremation, we study the evolution of bovine bone structure and chemistry as a function of heating temperature and time. Specifically, we apply all above mentioned analytical methods to the same unheated and heated bone material to allow a direct comparison of the obtained results. Furthermore, we analyse the gaseous reaction products during bone decomposition by combining Thermogravimetric Analysis with Fourier Transform Infrared Spectroscopy (TGA-FTIR).

Bone is a hierarchically structured composite material constituted of carbonated apatite nanocrystals mineralizing collagen (type I) microfibrils (Weiner et al., 1999; Fratzl et al., 2004). Secondary organic components are non-collagenous proteins such as phosphoproteins, which are considered to play an important role in bone mineralization (Rho et al., 1998; Olszta et al., 2007). Analyses on human bone revealed that it contains about 20–28% organics and about 8% water (bound to both, collagen and mineral) (Lim, 1975; LeGeros, 1991; Elliott, 2002). Biological apatite composition is chemically more complex than stoichiometric hydroxyapatite  $\text{Ca}_5(\text{PO}_4)_3(\text{OH})$  and can be approximated as  $(\text{Ca},\text{Mg},\text{Na}, \text{vacancy})_5(\text{PO}_4, \text{HPO}_4, \text{CO}_3)_3(\text{CO}_3, \text{H}_2\text{O}, \text{OH}, \text{F}, \text{Cl} \text{etc.})$  (Montel et al., 1981; Elliott, 1994; Wilson et al., 1999; Elliott, 2002; Pan and Fleet, 2002). Moreover, the chemical composition changes with both species and type of bone and is influenced by diet, physical activity and age (Bilz and Pellegrino, 1983; Driessens and Verbeeck, 1990; Rodríguez-Navarro et al., 2018). Carbonate content in bone mineral was determined between 5 and 8 wt% and either substitutes in the  $\text{OH}^-$  channel site (A-type substitution) or substitutes a tetrahedral  $\text{PO}_4^{3-}$  group (B-type substitution) of the apatite structure (LeGeros et al., 1969; Rey et al., 1990; Wopenka and Pasteris, 2005; Yi et al., 2013). In bone apatite, most of the carbonate substitutes are located at the phosphate-site rather than in the  $c$ -axis channel-site (Elliott, 2002). In this study we refer to bone mineral as "bioapatite". As previous studies showed, heating at low temperatures from 100 °C already induces small changes of the bioapatite structure (Harbeck et al., 2011). After Piga et al. (2009), Schmahl et al. (2017) and Greiner et al. (2018) recrystallization of the bioapatite and crystallite growth notably sets in from 600 °C onwards. In this study, we aim to narrow both, the temperature range and the role of heating time in order to specify the conditions where hydroxyapatite crystallization sets in. Moreover, we aim to gain a deeper knowledge on the decomposition process as well as structural and chemical changes in bone during thermal heat treatment.

## 2. Materials and methods

Pieces of compact bone were cut from the diaphysis of a fresh bovine femur and residuals of flesh, bone marrow and cancellous bone were mechanically removed. Subsequently, the bones were defatted for

five days with diethylether in a Soxhlet extractor which facilitates the grinding process. Fat residues on the bone surface were mechanically removed afterwards.

All heating experiments were carried out in a muffle furnace under oxidising conditions. Ten bone pieces were heated at temperatures ranging from 100 °C to 1000 °C (steps of 100 °C) for 150 min. In addition, six bone pieces were incinerated at 650 °C and six bone pieces at 700 °C for 10, 20, 30, 40, 50 and 60 min each. After incineration, the samples were finally homogenized to a fine powder and passed through a sieve with a mesh size of 100 µm to obtain a smooth sample surface for X-ray measurements.

X-ray diffractograms were measured on a General Electric 3003 powder diffractometer in Bragg-Brentano reflection geometry.  $\text{Cu-K}_{\alpha 1}$  radiation was selected with a focusing monochromator in the primary beam. An exposure time of 1000s on a 1D-Meteor detector was chosen, which resulted in a data collection time of 5 h for a diffractogram from 10 to 110° 2θ.

All samples were mixed with NIST 660b  $\text{LaB}_6$  as an internal standard between 2 and 5 wt% depending on the sample. The instrumental resolution function was experimentally determined using the internal standard. For data evaluation and Rietveld refinement (Rietveld, 1969) the FULLPROF code (Rodríguez-Carvajal, 1993; Rodríguez-Carvajal and Roisnel, 2004) was applied and we chose a hexagonal symmetry model of carbonated apatite (Wilson et al., 2004) for refinement. In the literature bone apatite is frequently sketched as platelet-shaped (e.g. Etok et al., 2007; Landis and Jacquet, 2013) due to the hexagonal or near-hexagonal (e.g. Ikoma and Yamazaki, 1999; Enzo et al., 2007; Tonegawa et al., 2010) metrics of the unit cell. The  $a$ - and  $b$ -axis cannot be distinguished in powder diffraction as the corresponding peaks exactly overlap. Therefore, crystallite size analysis by X-ray diffraction obtains only an average size for the directions perpendicular to the  $c$ -axis.

We used the Thompson-Cox-Hastings method for convolution of instrumental resolution with anisotropic size and isotropic microstrain broadening (Thompson et al., 1987). The low-angle part (10–12°) was excluded due to difficulties in describing small angle scattering contributions, such that the 010 reflection was not included in the refinement. We encountered persistent problems in modelling anisotropic line broadening in full-profile Rietveld refinement. Therefore, we finally determined the crystallite size in  $c$ -direction independently by a precise fit of the profile of the 002 reflection only, following the same Thompson-Cox-Hastings convolution procedures in FullProf as described for the full profile analysis.

Infrared spectra of the original and heat-treated bone mineral were measured on a Bruker Equinox FTIR instrument with a resolution of 4  $\text{cm}^{-1}$  and with 128 scans, resulting in a 2 minute acquisition time per sample. 1.4 mg of sample powder were mixed with 200 mg of KBr in a mortar, pressed to a pellet and subsequently measured. An analysis of the spectral decomposition in the range from 450 to 750  $\text{cm}^{-1}$  was performed that resulted in seven bands. Every bandshape was fitted with a combination of a Gaussian and a Lorentzian sum function for peak height and width, center position and peak area.

To study its thermal decomposition we heated the bone material in air atmosphere, by using a Shimadzu TGA-50H thermogravimetric analyzer equipped with a Mettler-Toledo AX26 Delta Range microbalance. The temperature was raised from 25 up to 950 °C at a heating rate of 20 °C/min. FTIR data from the gaseous reaction products were collected at regular time intervals of 1 min.

## 3. Results

### 3.1. Bone colour

The colour of bone changes in the course of thermal exposition. It was monitored by eye for a comparison with previously published observations and with the XRD and FTIR data.

**Table 1**

Bone colour observed for unheated bone and heat-treated bone for 150 min from 100 to 1000 °C under oxidising conditions.

Temperature (°C)	untreated	100	200	300	400	500
Colour	white-beige	white-beige	grey-brown	brown	grey-beige	light grey
Temperature (°C)	600	700	800	900	1000	
Colour	grey-white	white	white	white	white	

Unheated bone appears in a white-beige colour. At a temperature of about 300 °C bone colour changes to brown, appears grey-white at around 600 °C, and remains white at temperatures above 700 °C (Table 1).

Bone colour also changed dependent on the heating time periods. At 650 °C, the colour remains e.g. black after 10 min, and grey after 60 min incineration. In comparison, at 700 °C bone colour appeared black after 10 min heating, whereas it appears light grey after 60 min (Table 2).

### 3.2. X-ray diffraction

Fig. 1a shows a selected section of the X-ray powder diffraction patterns (24–36° 2θ range) of unheated bone and bones heated at different temperatures (100, 200, ... 1000 °C) for 150 min. The untreated bone mineral displays extremely broadened diffraction peaks due to its nanocrystalline nature. With increasing temperature up to 600 °C only a slight sharpening of the overlapping 121, 112 and 030 reflections can be observed while the 002 reflection, corresponding to the crystallographic c-axis of the crystallites, displays fairly the same broadening as for untreated bone or bone treated at lower temperatures. The diffraction pattern sharpens considerably from 700 °C upwards. The region of 31.5–33° 2θ showing overlapping peaks below 700 °C reveals clearly distinct 121, 112 and 030 reflections after treatment at temperatures of 700 °C or higher.

From 800 °C onwards, an additional mineral phase, which could be identified as buchwaldite, CaNaPO<sub>4</sub>, (Ben Amara et al., 1983; Piga et al., 2018), appears (Fig. 2b). According to the Rietveld refinement the bovine bone heat-treated at 1000 °C contains around 3 wt% of buchwaldite (Fig. 2). No lime (CaO) (Smith and Leider, 1968) could be

detected in our analyses (Fig. 1b).

Our Rietveld refinements of unheated and heat-treated bone show a good agreement between observed and calculated diffraction profiles (see selected sections from 24 to 40° 2θ in Fig. 3). Whole powder pattern refinements are shown in Fig. A1.

The evolution of the lattice parameters  $a$  ( $=b$ ) and  $c$  as measured at room temperature after thermal treatment for 2.5 h at each temperature is displayed in Fig. 4a. The lattice parameter  $c$  considerably increases with treatment from 100 to 200 °C, then decreases when heat-treated at 300–700 °C. From 700 to 1000 °C lattice parameters slightly increase but vary by only six Rietveld refinement standard deviations. Crystallite size increases only slightly up to 600 °C and rises dramatically at 700 °C (Fig. 4b).

Unit cell volume increases with heating at 200 °C, steadily decreases at 300–700 °C and slightly increases again from 700 °C along with the marked increase in crystallite size (Fig. 4b).

Since we could observe a significant structural change in bone mineral between 600 and 700 °C we focussed on this temperature range and shortened the heating periods to study not only the temperature- but also the time-dependence of bone crystallinity during incineration.

The X-ray diffractograms (only 24–36° 2θ range shown in Fig. 5a) of bovine bone incinerated at 650 °C for 10–60 min depict a steady narrowing of the 121, 112, 030 and 022 reflections with increasing heating time; even though, a still broad peak shape is observed after 60 minutes heating (Fig. 5a).

X-ray diffractograms of bovine bone heat-treated at 700 °C from 10 to 60 min show broad diffraction peaks from 10 to 30 min heating time, whereas reflections in the 31.5–33° 2θ range become considerably better defined after 30 minutes heating when compared to 650 °C (Fig. 5a,b). Diffraction peaks of bone mineral after 40–60 minutes heating are dramatically sharper than peaks after 30 minutes heating at 700 °C (Fig. 5b).

Rietveld refinement results display more clearly the differences in crystallite size evolution when comparing 650 and 700 °C (Fig. 6a,b). At 650 °C, lattice parameters  $a$  and  $c$  decrease steadily with progressing heating time, therefore the unit cell volume decreases as well (Fig. 6a,b). Crystallite sizes in  $a$ - and  $c$ -direction increase steadily with elapsed heating time, after 60 minutes heating at 650 °C apatite

**Table 2**

Bone colour observed for heat-treated bone at 650 and 700 °C from 10 to 60 min under oxidising conditions.

	10 min	20 min	30 min	40 min	50 min	60 min
650 °C	Black	Black	Black	Black-grey	Black-grey	Grey
700 °C	Black	Black	Black-grey	Grey	Light grey	Light grey

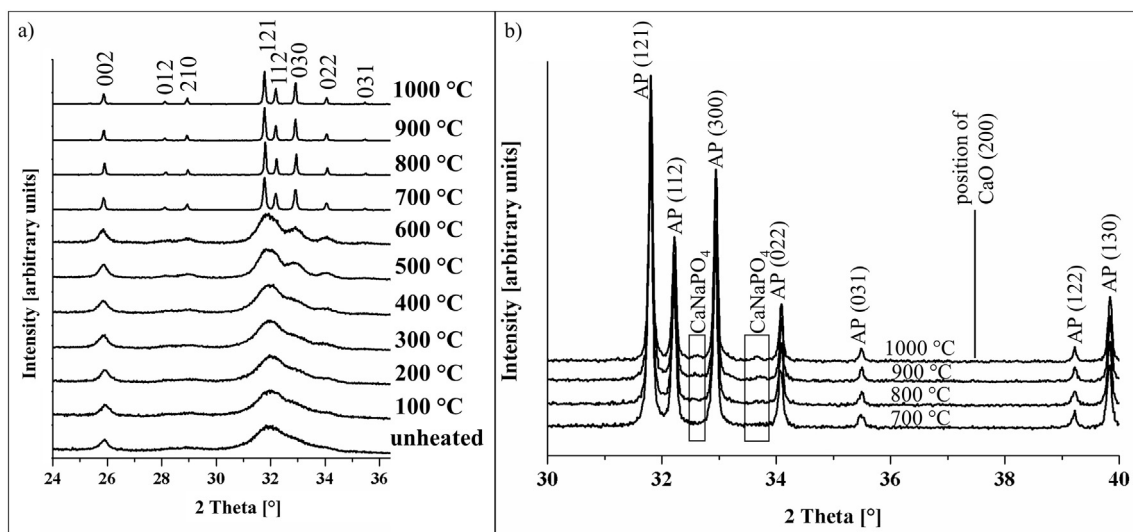


**Fig. 1.** (a) Sections of X-ray diffraction patterns ( $24\text{--}36^\circ 2\theta$ ) of unheated and heat-treated bone from 100 to 1000 °C; (b) XRD diffractograms ( $30\text{--}40^\circ 2\theta$ ) of bone heat-treated at 700, 800, 900 and 1000 °C. Corresponding phases are indicated, the position expected for the most prominent peak of CaO (200) is also pointed out. Note the emerging buchwaldite peaks from 800 °C (indicated with black rectangles).

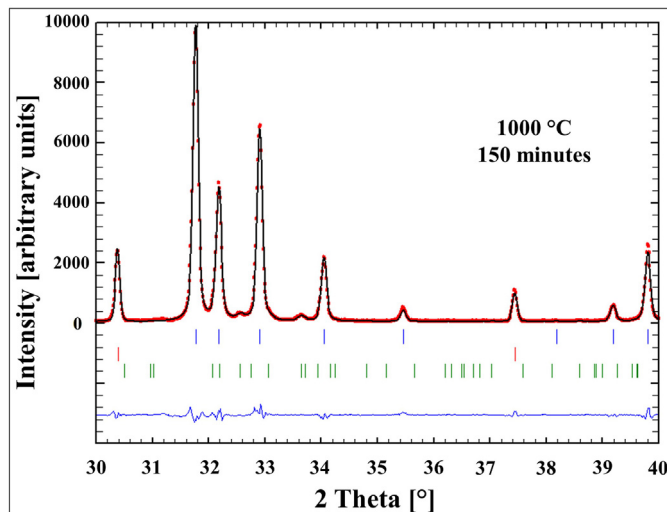


**Fig. 2.** Rietveld refinement ( $30\text{--}40^\circ 2\theta$ ) of bovine bone heat-treated at 1000 °C, 150 minutes heating. Red dots, observed data points; black line, calculated XRD profile; bottom blue line, difference of observed and calculated data; green vertical bars, positions of diffraction peaks of buchwaldite; red vertical bars, positions of diffraction peaks of LaB<sub>6</sub> standard, blue vertical bars, positions of diffraction peaks of bone apatite. (For interpretation of the references to colour in this figure legend, the reader is referred to the web version of this article.)

crystallites display a size of 251 Å in *c*- and 187 Å in *a*-direction (Fig. 6b). A standard deviation of 5% for calculated crystallite sizes is generated according to multiple refinements with different initial values.

Bovine bone heat-treated at 700 °C shows a constant increase of the crystallite size in *a*- and *c*-direction up to 30 minutes incineration. With 40 minutes heating, we observe a relatively sudden and dramatic increase of crystallite size from 134 Å to 266 Å in *a*- and 205 Å to 392 Å in *c*-direction (Fig. 6d). Furthermore, lattice parameters decrease (Fig. 6c) with heating time up to 30 min (*a*-axis) and 40 min (*c*-axis) which in consequence leads to a shrinkage of the unit cell (Fig. 6d). After 40 minutes heating the *c*-axis remains constant, whereas the *a*-axis increases again from 30 to 40 min and remains stable until 60 minutes heating (Fig. 6d). After 60 minutes heat-treated at 700 °C apatite crystallites have a size of 467 Å in *c*- and 389 Å in *a*-direction (Fig. 6d).

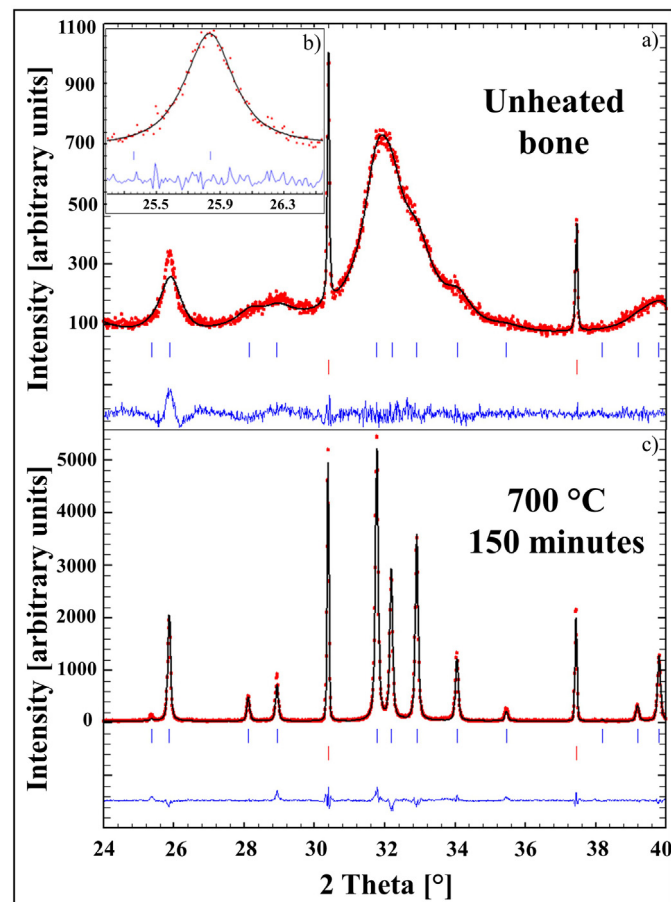


**Fig. 3.** Rietveld refinement of (a) unheated bovine bone ( $24\text{--}40^\circ 2\theta$ ), (b) the 002 reflection of unheated bovine bone ( $25.3\text{--}26.5^\circ 2\theta$ ) and (c) bone heat-treated at 1000 °C for 150 min ( $24\text{--}40^\circ 2\theta$ ). Red dots, observed data points; black line, calculated XRD profile; bottom blue line, difference of observed and calculated data; red vertical bars, positions of diffraction peaks of LaB<sub>6</sub> standard, blue vertical bars, positions of diffraction peaks of bone apatite. (For interpretation of the references to colour in this figure legend, the reader is referred to the web version of this article.)

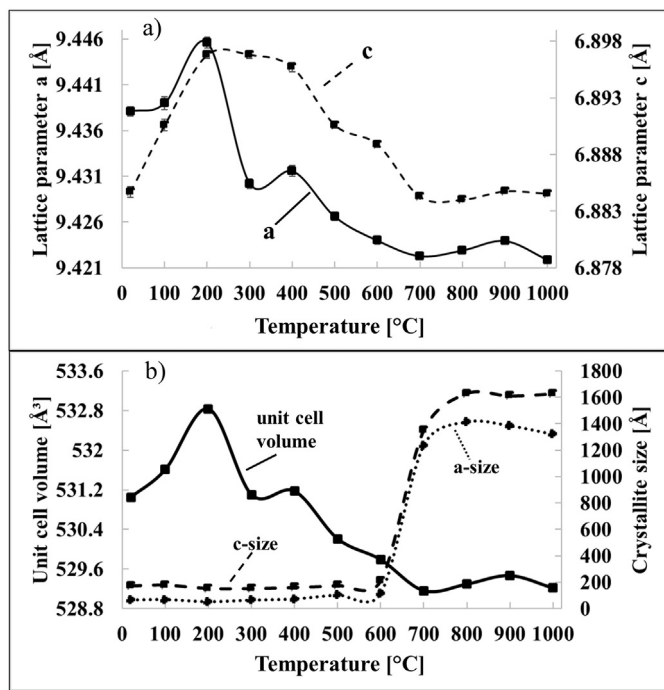


**Fig. 4.** (a) Lattice parameters  $a (=b)$  (solid line) and  $c$  (dashed line) of bone mineral, untreated and heat-treated from 100 to 1000 °C for 150 min; (b) Crystallite sizes in  $a$ -direction (dotted line) and  $c$ -direction (dashed line) and unit cell volume (solid line) of bone mineral heat-treated from 100 to 1000 °C for 150 min. The standard deviation for crystallite sizes is estimated as 5%.

### 3.3. FTIR

A comparison of IR spectra of untreated bone and bone heat-treated at different temperatures is shown in Fig. 7. Characteristic phosphate group vibrational bands at 470–480 cm<sup>-1</sup> ( $\nu_2\text{PO}_4^{3-}$ ), 500–750 cm<sup>-1</sup> ( $\nu_4\text{PO}_4^{3-}$ ), ~962 cm<sup>-1</sup> ( $\nu_1\text{PO}_4^{3-}$ ) and 980–1120 cm<sup>-1</sup> ( $\nu_3\text{PO}_4^{3-}$ ) could be identified according to Raynaud et al. (2002) and Destainville et al. (2003). Characteristic absorption bands at 873–879 cm<sup>-1</sup> (shifting to higher wavenumbers with heat treatment) and

1400–1458 cm<sup>-1</sup> were attributed to  $\nu_2\text{CO}_3^{2-}$  and  $\nu_3\text{CO}_3^{2-}$  (Rey et al., 1989; Rey et al., 1990; Fleet, 2009; Grunenwald et al., 2014). Carbonate band intensity begins to decrease continuously from 400 °C with increasing temperatures, and the carbonate bands disappear almost completely when bone is incinerated at 1000 °C. The untreated bovine bone spectrum shows broad H<sub>2</sub>O absorption bands from ~3000–3600 cm<sup>-1</sup> (Brubach et al., 2005). With heat treatment, these peaks lose intensity and disappear in the spectra of bone treated at 700 °C and higher.

At 200 °C heating, a subtle shoulder at 3570 cm<sup>-1</sup> appears which can be attributed to the OH<sup>-</sup> stretching mode (González-Díaz and Hidalgo, 1976; González-Díaz and Santos, 1977; Vandecandelaere et al., 2012), whereas the OH<sup>-</sup> libration mode at ~632 cm<sup>-1</sup> (Destainville et al., 2003) only becomes visible as a small shoulder at 400 °C heating (Fig. 7). However, both OH<sup>-</sup> signals just emerge when bone gets heat-treated and they are absent in the spectra of unheated bone. For samples treated at 700 °C or higher the OH<sup>-</sup> signals increase pronouncedly and become well-differentiated. Organic compounds like amids (~1540–1750 cm<sup>-1</sup>) show high peak intensities in the spectra of unheated bone and are barely visible in the sample treated at 400 °C; they diminish completely above 400 °C (Fig. 7).

FTIR spectral decomposition in the 450–750 cm<sup>-1</sup> range was based on seven peaks ( $\nu_2\text{PO}_4^{3-}$ , HPO<sub>4</sub><sup>2-</sup>, PO<sub>4</sub><sup>3-</sup>, PO<sub>4</sub><sup>3-</sup>, OH<sup>-</sup>, H<sub>2</sub>O) (Vandecandelaere et al., 2012) for both, unheated and heat-treated bone (Fig. 8a,b). The application of a protocol based on nine peaks for unheated bone to distinguish HPO<sub>4</sub><sup>2-</sup> and PO<sub>4</sub><sup>3-</sup> apatitic and nonapatitic environments did not converge to a reliable fit.

The  $\nu_2\text{PO}_4^{3-}$  and  $\nu_4\text{PO}_4^{3-}$  bands of unheated bone mineral show poor development of their spectral features and a large peak overlap, they become narrower with increasing temperature (Fig. 8a,b). The hydroxyl-libration peak at ~632 cm<sup>-1</sup> appears well-differentiated in heat-treated bone at 1000 °C, whereas it only exhibits a faint band in the spectral decomposition of unheated bovine bone (~621 cm<sup>-1</sup>). The HPO<sub>4</sub><sup>2-</sup> band shifts to higher wavenumbers with heat treatment (538 to 554 cm<sup>-1</sup>) and the peak area decreases (Fig. 8a,b).

### 3.4. Empirical crystallinity indices from XRD and FTIR data

For comparison with existing literature and to compare crystallinity indices obtained from different analytical methods, we provide popular empirical parameters such as the Crystallinity Index (CI) and the

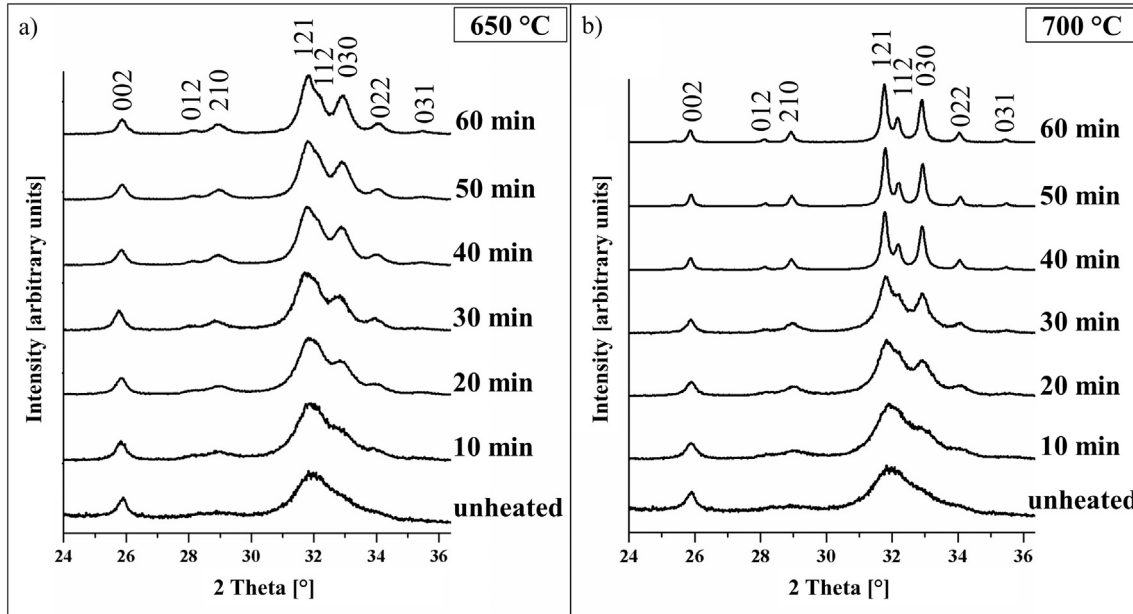


**Fig. 5.** X-ray diffraction patterns from the 24–36° 2θ range of unheated and heat-treated bone from 10 to 60 min (a) at 650 °C and (b) at 700 °C.

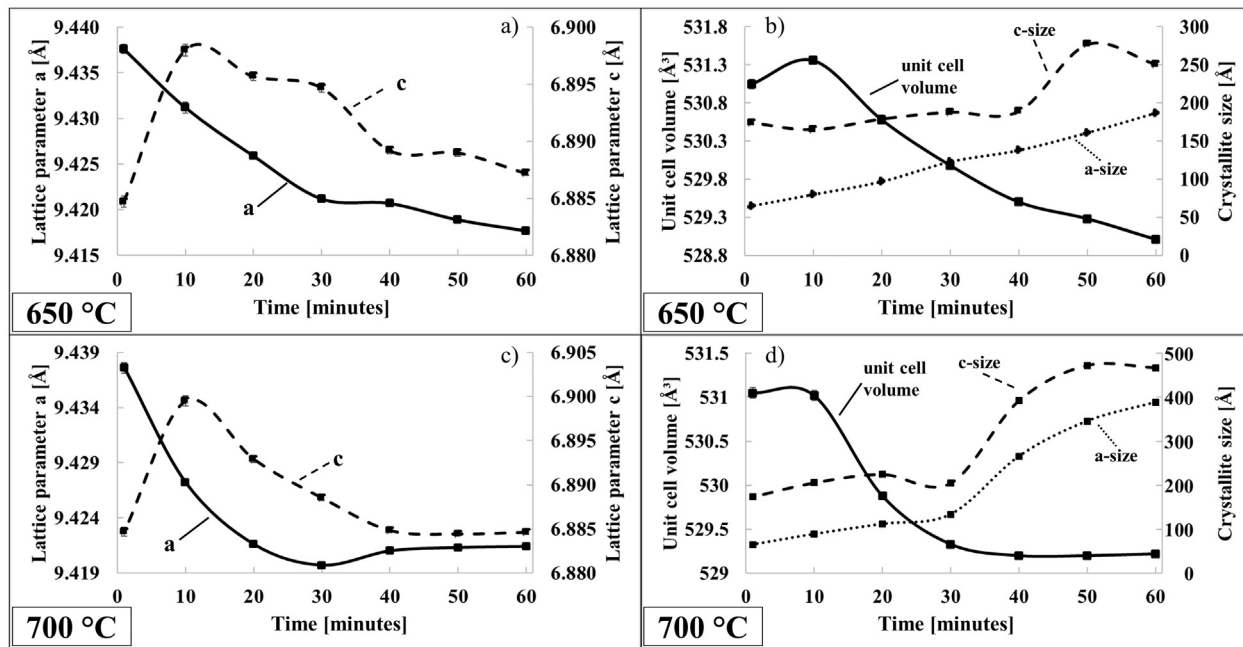


**Fig. 6.** (a) Lattice parameters  $a (= b)$  (solid line), and  $c$  (dashed line) of bone mineral, unheated and heat-treated at 650 °C for 10–60 min; (b) Crystallite sizes in  $a$ -direction (dotted line), and  $c$ -direction (dashed line) as well as unit cell volume (solid line) of bone mineral heat-treated at 650 °C for 10–60 min; (c) Lattice parameters  $a (= b)$  (solid line), and  $c$  (dashed line) of bone mineral, unheated and heat-treated at 700 °C for 10–60 min; (d) Crystallite sizes in  $a$ -direction (dotted line) and  $c$ -direction (dashed line) and unit cell volume (solid line) of bone mineral heat-treated at 700 °C for 10–60 min. The estimated standard deviation for crystallite sizes is 5%.

Infrared Splitting Factor (IRSF) (Table 3). The crystallinity index is a simple empirical measure of the degree of crystal organisation within bone mineral and involves a mathematical calculation using either XRD, Raman or FTIR data (e.g. Bonar et al., 1983; Shemesh, 1990; Weiner and Bar-Yosef, 1990; Person et al., 1995; Berna et al., 2004; Pucéat et al., 2004; Thompson et al., 2011). We calculated a CI (Table 3) from our XRD data according to Person et al. (1995): a baseline was taken between 24 and 38° 20 (Cu-K $\alpha$ 1 radiation) and the height (H) was measured between the average value at the top of a peak and the value of the valley separating it from the following peak (Person et al., 1995). These values of the 202, the 300 and the 112 reflection are added and divided by the height of the highest peak 211:

$$CI = \frac{\sum H[202], H[300], H[112]}{H[211]} \quad (1)$$

We calculated the IRSF (Table 3) measure of crystallinity from our

FTIR data according to Weiner and Bar-Yosef (1990) by adopting the following equation:

$$IRSF = \{A_{565} + A_{603}\}/A_{595} \quad (2)$$

with  $A_x$  being the absorbance corresponding to  $v_4\text{PO}_4$ , the two anti-symmetric bending vibration bands of phosphate at 565 and 603 cm $^{-1}$ , and the valley between them at 595 cm $^{-1}$  (Lebon et al., 2010). A baseline was drawn between 495 and 750 cm $^{-1}$  (Weiner and Bar-Yosef, 1990).

### 3.5. TGA-FTIR

The thermogram bovine bone heat-treated under air and its first derivative is shown in Fig. 9a. We observe four distinct stages of weight loss for bovine bone heat-treated under oxidising conditions, the weight

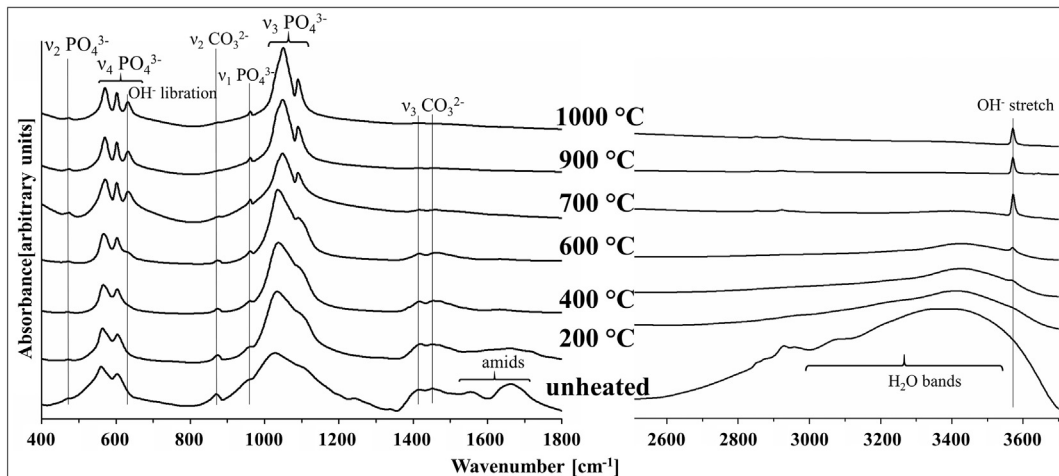


**Fig. 7.** Infrared absorbance spectra from 400 to 1800 cm $^{-1}$  (left side), and from 2500 to 3700 cm $^{-1}$  (right side) of untreated bone as well as of bone heat-treated for 200, 400, 600, 700, 900 and 1000 °C.

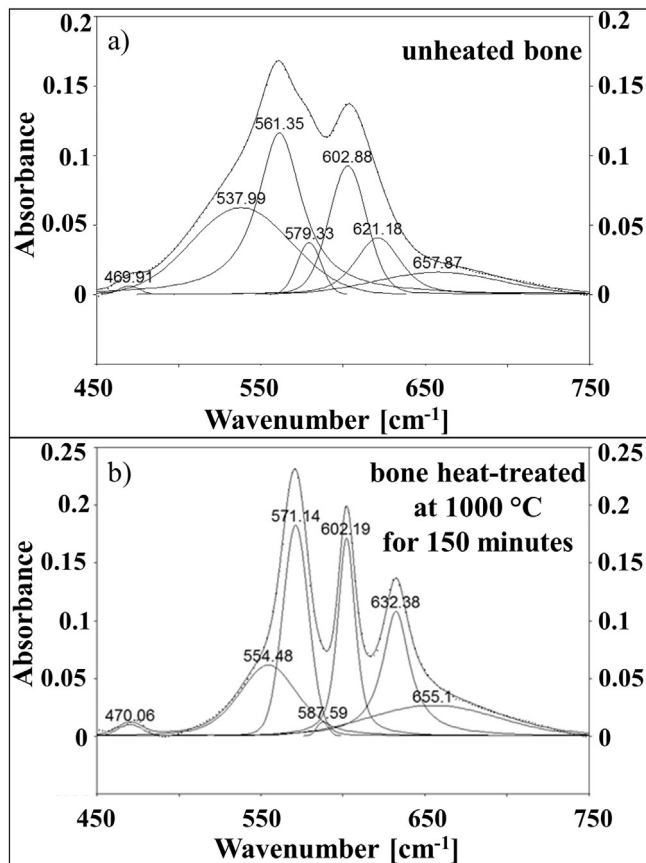


**Fig. 8.** Spectral decomposition of the FTIR signal of the  $\nu_2\text{PO}_4^{3-}$  and  $\nu_4\text{PO}_4^{3-}$  vibration bands of (a) unheated bone, and (b) bone heat-treated at 1000 °C for 150 min.

**Table 3**

Incineration temperature (time = 150 min), Crystallinity index calculated from XRD (CI) and FTIR (IRSF) data, respectively, and crystallite size in *a*- and *c*-direction (estimated standard deviation 5%) according to Rietveld refinements (see also Section 3.2 and Fig. 2b).

Temperature [°C]	CI	IRSF	<i>a</i> -size [Å]	<i>c</i> -size [Å]
Unheated	0.11	2.43	65	174
100	0.14	2.67	68	180
200	0.16	2.81	52	155
300	0.17	2.97	64	154
400	0.19	3.12	73	162
500	0.24	3.56	103	177
600	0.35	4.26	114	211
700	1.23	6.17	1236	1351
800	1.31	6.32	1413	1630
900	1.28	6.29	1384	1612
1000	1.30	6.96	1320	1628

loss for different temperature ranges is: 7.27% at 20–250 °C, 16.15% at 250–375 °C, 7.67% at 375–650 °C, and 2.01% at 650–950 °C.

The first derivative of the TGA curve ( $\Delta_{\text{mass}}/\Delta_{\text{temp}}$ ) was calculated to determine the precise temperature ranges of bone weight loss. We found well-defined peaks for bovine bone heat-treated in air at around 113, 352, 466, 770 and 812 °C. The most prominent peak and therefore the largest weight loss occurs between 300 and 400 °C.

Selected FTIR spectra of the gaseous reaction products of bovine bone heat-treated under air atmosphere are shown in Fig. 10. Distinct  $\text{H}_2\text{O}$  and  $\text{CO}_2$  peaks emerge in the spectra at 122 °C and can still be observed in the spectra measured at 979 °C. CO bands at 2116 and 2177  $\text{cm}^{-1}$  emerge from about 300 °C and disappear around 550 °C.

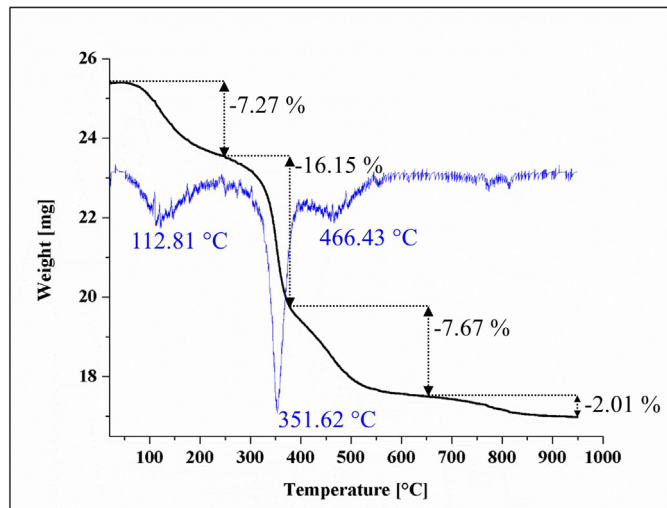


**Fig. 9.** TGA thermogram of bone heat-treated in atmosphere (black line) and its first derivative (blue line). (For interpretation of the references to colour in this figure legend, the reader is referred to the web version of this article.)

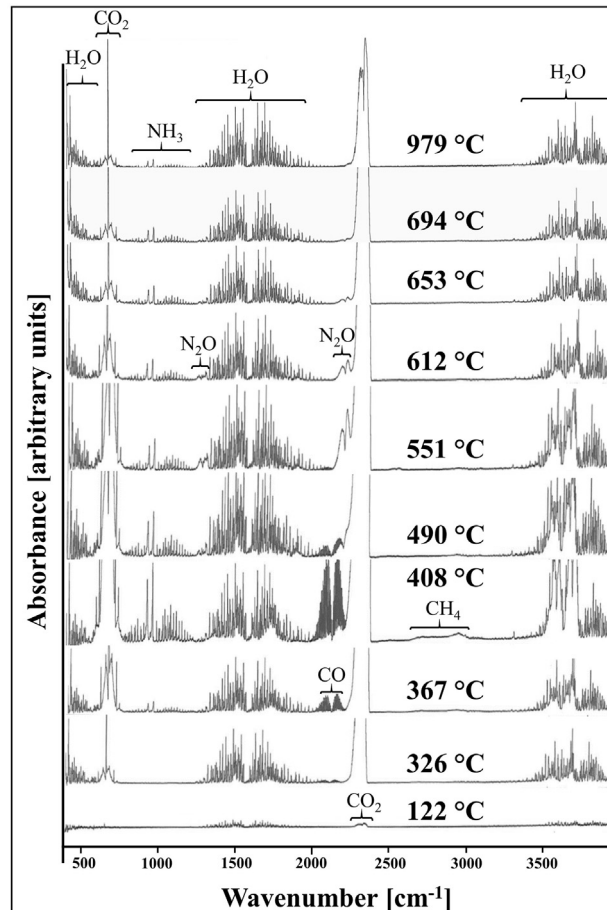


**Fig. 10.** FTIR spectra of gaseous reaction products of bone during TGA measurements in air (oxidising conditions).

$\text{N}_2\text{O}$  bands appear around 490 °C, show less intensity at 653 °C and disappear completely at higher temperatures.  $\text{NH}_3$  absorption bands appear first in the spectra measured at 367 °C, show highest intensity from 400 to 450 °C and show less intensity in the spectra taken at temperatures higher than 653 °C. These bands are produced by gases evolving from the thermal decomposition (pyrolysis) of the organic

components of bone (mainly collagen and non-collagenous proteins).

#### 4. Discussion

##### 4.1. Crystalline by-products during heat treatment

For heating at very high temperatures, lime ( $\text{CaO}$ ) is a likely decomposition product of bioapatite, and it was indeed reported by Piga et al. (2008, 2009). They detected around 3 wt% calcite in archaeological human bone finds and  $\text{CaO}$  after thermal treatment at 775 °C onwards (Piga et al., 2008), and explained it with the chemical reaction of carbonate thermal decomposition  $\text{CaCO}_3 \rightarrow \text{CaO} + \text{CO}_2$  in consequence of thermal treatment. In our diffractograms we found no evidence for  $\text{CaO}$ . However, we identified another crystalline phase: Buchwaldite ( $\text{CaNaPO}_4$ ), occurring from 800 °C and at higher temperatures as carbonate-free hydroxyapatite grows due to decomposition of the bioapatite. This can be explained with cortical bovine bone mineral containing about 1 wt% Na (Elliott, 2002).  $\text{CaNaPO}_4$  was also detected in a similar study by Etok et al. (2007) who investigated meat and bone meal (MBM), a product produced from wastes of the meat industry. In heat-treated MBM, however,  $\text{CaNaPO}_4$  was already discernible at 500 °C. These authors also report the presence of KCl and NaCl from 500 °C and  $\beta$ -TCP occurring at 900 °C. These non-conformances may be due to differences in the materials (Na, K, and Cl contents, species, initial composition of the bioapatite) and/or the heating process.

##### 4.2. Bone mineral is not hydroxyapatite

Original, untreated bone XRD patterns show broad diffraction peaks (Fig. 1a) due to the nanometric size of the apatite crystallites. The original bone apatite is clearly no hydroxylapatite as proven by the lack of  $\text{OH}^-$  bands (Figs. 7 and 8a). The high intensity of the carbonate and  $\text{H}_2\text{O}$  vibration bands clearly indicate that bone apatite instead is a carbonate-hydro-apatite (Fig. 7). Similar conclusions were made by Pasteris et al. (2004) using raman spectroscopy, Rey et al. (1989, 1995) and Mkukuma et al. (2004) using infrared spectroscopy, Rey et al. (1995) using solid state NMR and Loong et al. (2000) using inelastic neutron scattering.

Following Fleet (2009) and Rey and co-workers (Rey et al., 1989, 1990; El Feki et al., 1991; Vandecandelaere et al., 2012), the position of the  $\nu_2\text{CO}_3^{2-}$  peak at  $\sim 873 \text{ cm}^{-1}$  of unheated and heat-treated bone samples up to 600 °C can be attributed to the B-type substitution, from 700 °C onwards we locate this peak at  $878 \text{ cm}^{-1}$  which is attributed to the A-type substitution. Following the previously mentioned authors, the shift of the  $\text{HPO}_4^{2-}$  band can be attributed to “non-apatitic  $\text{HPO}_4^{2-}$ ” and “apatitic  $\text{HPO}_4^{2-}$ ” at  $538 \text{ cm}^{-1}$  and  $554 \text{ cm}^{-1}$ , respectively.

With extended heating treatment (temperature and time) under oxidising conditions, the diffraction peaks of the bioapatite get sharper. At the same time, the intensity of the carbonate infrared signals decrease while the intensity of the  $\text{OH}^-$  infrared signals increase, most pronounced between 600 and 700 °C (Fig. 7). As temperatures rise, the  $\text{OH}^-$  stretching occurs from 200 °C and increases with higher temperatures (Fig. 7). This leads to the conclusion that the carbonate-hydro-apatite reacts to hydroxyapatite with heat treatment according to the formula  $[\text{CO}_3]^{2-} + \text{H}_2\text{O} \rightarrow \text{CO}_2 \uparrow + 2\text{OH}^-$ . This was also observed by Cho et al. (2013) and Ooi et al. (2007) investigating bovine bone xenografts and Holcomb and Young (1980) studying the thermal decomposition of human tooth enamel. As the material approaches stoichiometric chemistry, the loss of carbonate and water and their replacement by  $\text{OH}^-$  in the structure lead to a decrease of unit cell parameters (Figs. 4b, 6d). This reaction is correlated with a growth of the crystallites, which is even more pronounced at temperatures starting from 700 °C (Fig. 4b). We attribute the weight loss at 650 °C and higher temperatures to the decomposition of the carbonate (Fig. 9), which results in a carbonate content of around 4 wt% for the original

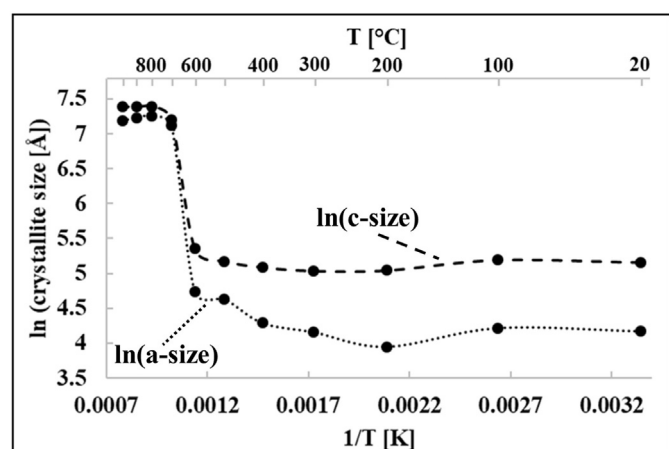


Fig. 11. Arrhenius graph of the crystallite size in  $a$ - and  $c$ -direction.

bioapatite in a bovine femur.

##### 4.3. Combustion of organic components in bone leads to enhanced crystallite growth

If we assumed that the observed acceleration of crystallite growth at high temperatures is simply a thermally activated process, we would expect the crystallite growth rate  $r$  to follow a Boltzmann law as.

$$r = r_0 \exp - \frac{E_A}{k_B T} \quad (3)$$

where  $E_A$  is the activation energy,  $k_B$  is the Boltzmann constant and  $T$  is the temperature. Crystallite size  $K$  after time  $t$  is

$$K = r t = t r_0 \exp - \frac{E_A}{k_B T} \quad (4)$$

Thus, for the isochronic experiment ( $t = 150 \text{ min}$ ) an Arrhenius law

$$\ln(K) = \ln(t) + \ln(r_0) - \left( \frac{E_A}{k_B} \right) \left( \frac{1}{T} \right) \quad (5)$$

would result (if the heating and cooling periods can be neglected). Fig. 11 plots  $\ln(K)$  vs.  $1/T$ . In a simple thermally activated process a straight line would be expected. It can be clearly seen, that, instead, a large discontinuity occurs between 600 and 700 °C, i.e. the temperature where the combustion of the organic material is complete.

Considering the stages of weight loss, we attribute the first stage from 20 to around 250 °C with the most prominent peak reaction rate at  $\sim 113^\circ\text{C}$  (Fig. 9c) to the evaporation of water. Decomposition of the collagen molecules and non-collageneous proteins mainly occurs from about 300 °C (see considerable weight loss between 300 and 400 °C in Fig. 9 and emerging  $\text{CO}_2$ ,  $\text{N}_2\text{O}$ , and  $\text{NH}_3$  absorption bands in the gaseous products spectra from 367 °C in Fig. 10). HCN, HNCO and  $\text{NH}_3$  are main pyrolysis products of proteins. CO,  $\text{CO}_2$ ,  $\text{H}_2\text{O}$  and  $\text{N}_2\text{O}$  are their secondary reaction products due to combustion and reaction with air (Wargadalam et al., 2000; Hansson et al., 2004). For temperatures higher than about 650 °C, CO and  $\text{N}_2\text{O}$  signals disappear and  $\text{NH}_3$  bands are less intense in the FTIR spectra (Fig. 10). This leads to the conclusion that the majority of proteinous components (collagen and non-collageneous proteins) had been removed from the bone when this temperature was reached. Holden et al. (1995) investigating heat-treated human bones by electron microscopy imaging also reported the complete removal of organic compounds in the bone tissue at temperatures around 600 °C. If the enhanced crystallite growth was simply driven by  $T$  as a thermally-activated process, the Arrhenius graph of crystallite sizes and temperature would show a linear behaviour (Fig. 11). Hence, we conclude that the noticeable acceleration of crystallite growth which we observed for samples heat-treated at 700 °C for

30 min and after (Figs. 4b and 6d) takes place because the crystallites are no longer protected by organic residues coating so they can grow unhindered.

#### 4.4. Concluding from bone colour and crystallite size to cremation temperature is not trivial

The fact that the bone reaction process is not only temperature- but also time-dependent complicates the assignment of a cremation temperature to changes observed in bone characteristics (i.e. colour). There are visible changes of bone colour with progressing heating time: at 700 °C we observe black-coloured samples for 10 min, black-grey for 30, grey for 40 and light grey for 50 and 60 min. After 150 minutes heating at 700 °C, the bone material appears white. Samples heat-treated at 650 °C appear black from 10 to 30 minutes heating time, black-grey for 40 and 50 min, and remain grey after 60 minutes heating time. After Wahl (1982), bone remains grey at incineration temperatures around 550 °C, milky-white from 650 to 700 °C and white above 800 °C. After Harbeck et al. (2011), bones that were exposed to temperatures between 500 and 600 °C show a black-grey colour and remain white when burnt at 700 °C or higher. In conclusion, we show that an estimation of cremation temperature from the colour of archaeological incinerated bone finds is not straight forward at all, as bones incinerated at 700 °C for 30 min have quite the same colour as bones burnt for 40 and 50 min at 650 °C and as bones heat-treated between 500 and 600 °C.

In the same manner, one needs to be careful when estimating cremation temperature from bone crystallite size data. Our results show that bone heat-treated at 100 °C for 150 min displays similar crystallite sizes (68 Å in *a*- and 180 Å in *c*-direction) as bone treated at 650 °C for 10 min (80 Å in *a*- and 165 Å in *c*-size).

By comparing 650 °C and 700 °C, the same trend for lattice parameters and – in consequence - unit cell parameters is observable. Lattice parameters *a* and *c* decrease, therefore the unit cell shrinks which is coupled with an increase of the crystallite size (Fig. 6). However, after 30 minutes heating the 50 °C temperature difference and the removal of the organic components or their residues, respectively, shows its impact as crystallites grow distinctively faster at 700 °C after 30 minutes heating which we ascribe to a progressive recrystallization reaction of

bioapatite to hydroxyapatite.

After 30 minutes heating at 700 °C, decomposition products (essentially carbon, which is responsible for the black colour of samples incinerated for shorter times) of organics such as collagen, have almost disappeared and the apatite crystallites can grow without being hindered by organic compounds or their residues which separate and coat the crystallites.

In conclusion, there are well-defined changes in bone chemistry, structure and crystallinity during thermal treatment. The bone bioapatite unit cell shrinks with increasing temperature and the crystallite size increases dramatically after organic matter is lost. The original bone mineral is carbonated apatite and it reacts/recrystallizes to hydroxyapatite in consequence of heat treatment. Moreover, an additional phase (buchwaldite, NaCaPO<sub>4</sub>) forms from 800 °C onwards.

Our study assesses the results obtained from a combination of analytical methods which are typically applied and approved to determine bone cremation temperatures. This combination gives a more complete understanding of the complex processes taking place during bone cremation. The described changes in the state of the bone mineral are not only dependent of temperature but also on time. Thus, care must be taken when deducing the defined temperature cremated bone finds were exposed to.

#### Declaration of Competing Interest

The authors declare that they have no conflict of interest.

#### Acknowledgement

We would like to thank the reviewers for their valuable comments and suggestions, Brittany Foley for proof reading and the editors for handling the manuscript.

#### Funding

This work was supported by the German Research Foundation (DFG) in Forschergruppe FOR1670 [grant numbers Schm930/12-1 and Gr 959/20-1,2].

## Appendix A

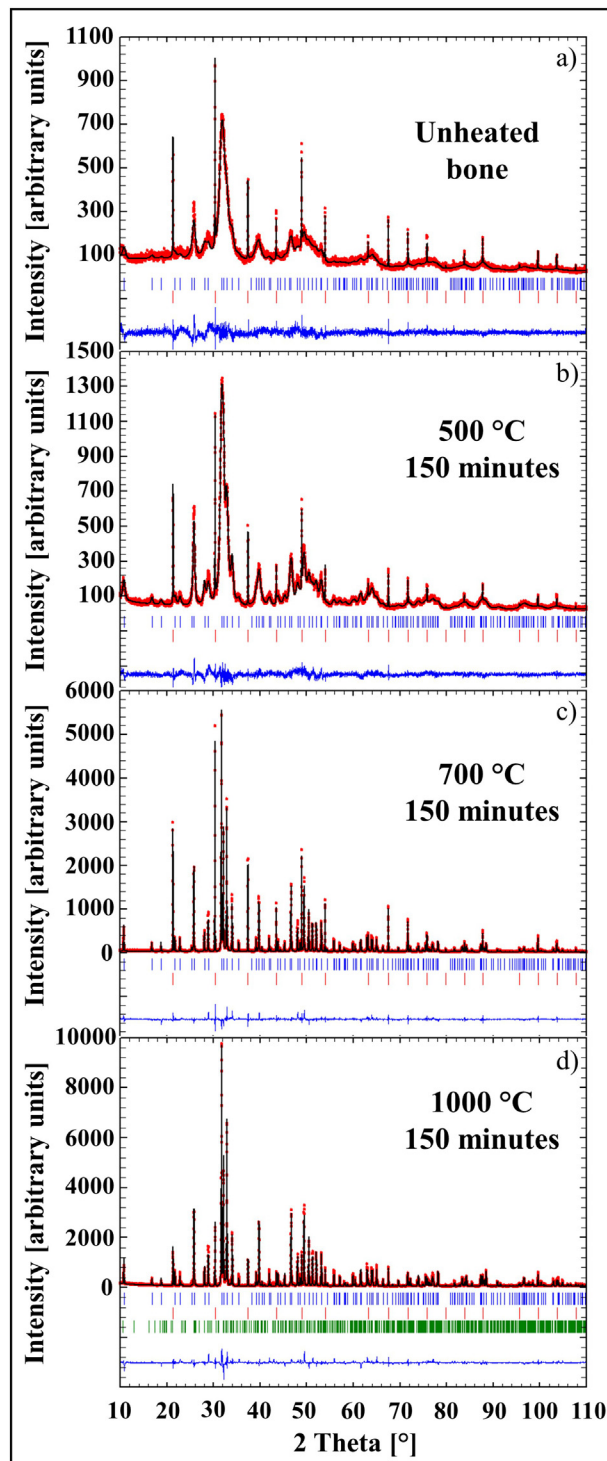


**Fig. A1.** Rietveld refinement (10–110° 2θ) of (a) untreated bovine bone; (b) bone heat-treated at 500 °C for 150 min; (c) bone heat-treated at 700 °C for 150 min; bone heat-treated at 1000 °C for 150 min. Red dots, observed data points; black line, calculated XRD profile; bottom blue line, difference of observed and calculated data; green vertical bars, positions of diffraction peaks of buchwaldite; red vertical bars, positions of diffraction peaks of LaB<sub>6</sub> standard, blue vertical bars, positions of diffraction peaks of bone apatite.

## References

- Ben Amara, M., Vlasse, M., le Flem, G., Hagenmuller, P., 1983. Structure of the low-temperature variety of calcium sodium orthophosphate, NaCaPO<sub>4</sub>. *Acta Cryst* 39, 1483–1485.  
 Bennett, J.L., 1999. Thermal alteration of buried bone. *J. Archaeol. Sci.* 26, 1–8.  
 Berna, F., Matthews, A., Weiner, S., 2004. Solubilities of bone mineral from archaeological sites: the recrystallization window. *J. Archaeol. Sci.* 31, 867–882.  
 Biltz, R.M., Pellegrino, E.D., 1983. The composition of recrystallized bone mineral. *J. Dent. Res.* 62, 1190–1195.  
 Bonar, L.C., Roufosse, A.H., Sabine, W.K., Grynpas, M.D., Glimcher, M.J., 1983. X-ray

- diffraction studies of the crystallinity of bone mineral in newly synthesized and density fractionated bone. *Calcif. Tissue Int.* 35, 202–209.
- Bonucci, E., Graziani, G., 1975. Comparative thermogravimetric X-ray diffraction and electron microscope investigations of burnt bones from recent, ancient and prehistoric age. *Atti della accademia Nazionale dei Lincei, Rendiconti, classe die Scienze fisiche, matematiche e naturali* 59, 517–532.
- Brubach, J.B., Mermet, A., Filabozzi, A., Gerschel, A., Roy, P., 2005. Signatures of the hydrogen bonding in the infrared bands of water. *J. Chem. Phys.* 122, 184509.
- Cho, J.S., Kim, H.S., Um, S.H., Rhee, S.H., 2013. Preparation of a novel anorganic bovine bone xenograft with enhanced bioactivity and osteoconductivity. *J Biomed Mater Res B* 101B, 855–869.
- Destainville, A., Champion, E., Bernache-Assollant, D., Laborde, E., 2003. Synthesis, characterization and thermal behavior of apatitic tricalcium phosphate. *Mater. Chem. Phys.* 80, 269–277.
- Driessens, F.C.M., Verbeek, R.M.H., 1990. *Biominerals*. CRC Press, Boca Raton, Florida.
- Dunlop, J.M., 1978. Traffic light discoloration in cremated bones. *Med Sci Law* 18, 163–173.
- El Feki, H., Rey, C., Vignoles, M., 1991. Carbonate ions in apatites: infrared investigations in the  $\nu_4\text{CO}_3$  domain. *Calcif Tiss Int* 49, 269–274.
- Ellingham, S.T.D., Thompson, T.J.U., Islam, M., 2015. Thermogravimetric analysis of porosity changes and weight loss in incinerated bone. *Palaeogeogr. Palaeoclimatol. Palaeoecol.* 438, 239–244.
- Elliott, J.C., 1994. *Structure and Chemistry of the Apatites and Other Calcium Orthophosphates*. Elsevier, Amsterdam.
- Elliott, J.C., 2002. Calcium phosphate biominerals. *Rev. Mineral. Geochem.* 48, 427–453.
- Enzo, S., Bazzoni, M., Mazzarello, V., Piga, G., Bandiera, P., Melis, P., 2007. A study by thermal treatment and X-ray powder diffraction on burnt fragmented bones from tombs II, IV and IX belonging to the hypogeal necropolis of “Sa Figu” near Ittiri, Sassari (Sardinia, Italy). *J. Archaeol. Sci.* 34, 1731–1737.
- Etok, S.E., Valsami-Jones, E., Wess, T.J., Hiller, J.C., Maxwell, C.A., et al., 2007. Structural and chemical changes of thermally treated bone apatite. *J. Mater. Sci.* 42, 9807–9816.
- Fleet, M.E., 2009. Infrared spectra of carbonate apatites: v2-region bands. *Biomaterials* 30, 1473–1481.
- Fratzl, P., Gupta, H.S., Paschalidis, E.P., Roschger, P., 2004. Structure and mechanical quality of the collagen-mineral nano-composite in bone. *J. Mater. Chem.* 14, 2115–2123.
- Galeano, S., García-Lorenzo, M.L., 2014. Bone mineral change during experimental calcination: an X-ray diffraction study. *J. Forensic Sci.* 59, 1602–1606.
- González-Díaz, P.F., Hidalgo, A., 1976. Infrared spectra of calcium apatites. *Spectrochim. Acta A* 32, 631–635.
- González-Díaz, P.F., Santos, M., 1977. On the hydroxyl ions in apatites. *J. Solid State Chem.* 22, 193–199.
- Greiner, M., Kocsis, B., Heinig, M.F., Mayer, K., Toncalo, A., Grupe, G., Schmahl, W.W., 2018. Experimental cremation of bone: crystallite size and lattice parameter evolution. In: *Biomineralization: From Molecular and Nano-Structural Analyses to Environmental Science*. Springer, Singapore.
- Grunenwald, A., Keyser, C., Sautereau, A.M., Crubézy, E., Ludes, B., Drouet, C., 2014. Revisiting carbonate quantification in apatite (bio)minerals: a validated FTIR methodology. *J. Archaeol. Sci.* 49, 134–141.
- Grupe, G., Harbeck, M., McGlynn, G.C., 2015. *Prähistorische Anthropologie*. Springer, Berlin.
- Grupe, G., Grigat, A., McGlynn, G.C., 2017. Across the Alps in Prehistory. Springer International Publishing, pp. 75–104.
- Hansson, K.M., Samuelsson, J., Tullin, C., Åmand, L.E., 2004. Formation of HNCO, HCN and NH<sub>3</sub> from the pyrolysis of bark and nitrogen-containing model compounds. *Combust Flame* 137, 265–277.
- Harbeck, M., Schleuder, R., Schneider, J., Wiechmann, I., Schmahl, W.W., Grupe, G., 2011. Research potential and limitations of trace analyses of cremated remains. *Forensic Sci. Int.* 204, 191–200.
- Herrmann, B., 1977. On histological investigations of cremated human remains. *J. Hum. Evol.* 6, 101–103.
- Hiller, J.C., Thompson, T.J.U., Evison, M.P., Chamberlain, A.T., Wess, T.J., 2003. Bone mineral change during experimental heating: an X-ray scattering investigation. *Biomaterials* 24, 5091–5097.
- Holcomb, D.W., Young, R.A., 1980. Thermal decomposition of human tooth enamel. *Calcified Tissue Int* 31, 189–201.
- Holden, J.L., Clement, J.G., Phakey, P.P., 1995. Age and temperature related changes to the ultrastructure and composition of human bone mineral. *J. Bone Miner. Res.* 10, 1400–1409.
- Ikoma, T., Yamazaki, A., 1999. Preparation and structure refinement of monoclinic hydroxyapatite. *J. Solid State Chem.* 144, 272–276.
- Landis, W.J., Jacquet, R., 2013. Association of calcium and phosphate ions with collagen in the mineralization of vertebrate tissues. *Calcif. Tissue Int.* 93, 329–337.
- Lebon, M., Reiche, I., Frohlich, F., Bahain, J.J., Falgueres, C., 2008. Characterization of archaeological burn bones: contribution of a new analytical protocol based on derivative FTIR spectroscopy and curve fitting of the  $\nu_1\nu_3\text{PO}_4$  domain. *Anal. Bioanal. Chem.* 392, 1479–1488.
- Lebon, M., Reiche, I., Bahain, J.J., Chadeaux, C., Moigne, A.M., Fröhlich, F., Sémaire, F., Schwarzs, H.P., Falguères, C., 2010. New parameters for the characterization of diagenetic alterations and heat-induced changes of fossil bone mineral using Fourier transform infrared spectrometry. *J. Archaeol. Sci.* 37, 2265–2276.
- LeGeros, R.Z., 1991. *Calcium Phosphates in Oral Biology and Medicine*. Karger, Basel.
- LeGeros, R.Z., Trautz, O.R., Klein, E., LeGeros, J.P., 1969. Two types of carbonate substitution in the apatite structure. *Experientia* 25, 5–7.
- Lim, J.J., 1975. Thermogravimetric analysis of human femur bone. *J. Biol. Phys.* 3, 111–129.
- Loong, C.K., Rey, C., Kuhn, L.T., Combes, C., Wu, Y., Chen, S.H., Glimcher, M.J., 2000. Evidence of hydroxyl-ion deficiency in bone apatites: an inelastic neutron-scattering study. *Bone* 26, 599–602.
- Mamede, A.P., Vassalo, A.R., Piga, G., Cunha, E., Parker, S.F., Marques, M.P.M., Batista de Carvalho, L.A.E., Gonçalves, D., 2018. Potential of bioapatite hydroxyls for research on archaeological burned bone. *Anal. Chem.* 90, 11556–11563.
- Mukukuma, L.D., Skakle, J.M.S., Gibson, I.R., Imrie, C.T., Aspden, R.M., Hukins, D.W.L., 2004. Effect of the proportion of organic material in bone on thermal decomposition of bone mineral: an investigation of a variety of bones from different species using thermogravimetric analysis coupled to mass spectrometry, high-temperature X-ray diffraction, and Fourier transform infrared spectroscopy. *Calcif. Tissue Int.* 75, 321–328.
- Montel, G., Bonel, G., Heughebaert, J.C., Trombe, J.C., Rey, C., 1981. New concepts in the composition, crystallization and growth of the mineral component of calcified tissues. *J. Cryst. Growth* 53, 74–99.
- Munro, L.E., Longstaffe, F.J., White, C.D., 2007. Burning and boiling of modern deer bone: effects on crystallinity and oxygen isotope composition of bioapatite phosphate. *Palaeogeogr. Palaeoclimatol. Palaeoecol.* 249, 90–102.
- Munro, L.E., Longstaffe, F.J., White, C.D., 2008. Effects of heating on the carbon and oxygen-isotope compositions of structural carbonate in bioapatite from modern deer bone. *Palaeogeogr. Palaeoclimatol. Palaeoecol.* 266, 142–150.
- Nicholson, R.A., 1993. A morphological investigation of burnt animal bone and an evaluation of its utility in archaeology. *J. Archaeol. Sci.* 20, 411–428.
- Olszta, M.J., Cheng, X., Jee, S.S., Kumar, R., Kim, Y., Kaufmann, M.F., Douglas, E.P., Gower, L.B., 2007. Bone structure and formation: a new perspective. *Mater. Sci. Eng. R. Rep.* 58, 77–106.
- Ooi, C.Y., Hamdi, M., Ramesh, S., 2007. Properties of hydroxyapatite produced by annealing of bovine bone. *Ceram. Int.* 33, 1171–1177.
- Pan, Y., Fleet, M.E., 2002. Compositions of the apatite-group minerals: substitution mechanisms and controlling factors. *Rev. Mineral. Geochem.* 48, 13–49.
- Pasteris JD, Wopenka B, Freeman, Rogers K, Valsami-Jones E, van der Houwen JAM, Silva MJ (2004) Lack of OH in nanocrystalline apatite as a function of degree of atomic order: implications for bone and biomaterials. *Biomaterials* 25:229–238.
- Person, A., Bocherens, H., Saliège, J.-F., Paris, F., Zeitoun, V., Gérard, M., 1995. Early diagenetic evolution of bone phosphate: an X-ray diffractometry analysis. *J. Archaeol. Sci.* 22, 211–221.
- Person, A., Bocherens, H., Mariotti, A., Renard, M., 1996. Diagenetic evolution and experimental heating of bone phosphate. *Palaeogeogr. Palaeoclimatol. Palaeoecol.* 126, 135–149.
- Piga, G., Malgosa, A., Thompson, T.J.U., Enzo, S., 2008. A new calibration of the XRD technique for the study of archaeological burned human remains. *J. Archaeol. Sci.* 35, 2171–2178.
- Piga, G., Thompson, T.J.U., Malgosa, A., Enzo, S., 2009. The potential of X-ray diffraction in the analysis of burned remains from forensic contexts. *J. Forensic Sci.* 54, 534–539.
- Piga, G., Amarante, A., Makhoul, C., Cunha, E., Malgosa, A., Enzo, S., Gonçalves, D., 2018.  $\beta$ -Tricalcium phosphate interferes with the assessment of crystallinity in burned skeletal remains. *J. Spectrosc.* 2018, 1–10.
- Pucéat, E., Reynard, B., Lécyer, C., 2004. Can crystallinity be used to determine the degree of chemical alteration of biogenic apatites? *Chem. Geol.* 205, 83–97.
- Raynaud, S., Champion, E., Bernache-Assollant, D., Thomas, P., 2002. Calcium phosphate apatites with variable Ca/P atomic ratio I. Synthesis, characterisation and thermal stability of powders. *Biomaterials* 23, 1065–1072.
- Rey, C., Collins, B., Goehl, T., Dickson, I.R., Glimcher, M.J., 1989. The carbonate environment in bone mineral: a resolution-enhanced Fourier Transform Infrared Spectroscopy Study. *Calcif. Tissue Int.* 45, 157–164.
- Rey, C., Shimizu, M., Collins, B., Glimcher, M., 1990. Resolution-enhanced Fourier transform infrared spectroscopy study of the environment of phosphate ions in the early deposits of a solid phase of calcium-phosphate in bone and enamel, and their evolution with age. I: investigations in the  $\nu_4\text{PO}_4$  domain. *Calcif. Tissue Int.* 46, 384–394.
- Rey, C., Miquel, J.L., Facchini, L., Legrand, A.P., Glimcher, M.J., 1995. Hydroxyl groups in bone mineral. *Bone* 16, 583–586.
- Rho, J.Y., Kuhn-Spearing, L., Ziopoulos, P., 1998. Mechanical properties and the hierarchical structure of bone. *Med. Eng. Phys.* 20, 92–102.
- Rietveld, H.M., 1969. A profile refinement method for nuclear and magnetic structures. *J. Appl. Crystallogr.* 2, 65–71.
- Rodríguez-Carvajal, J., 1993. Recent advances in magnetic structure determination by neutron powder diffraction. *Physica B* 192, 55–69.
- Rodríguez-Carvajal, J., Roisnel, T., 2004. Line broadening analysis using FullProf\*: determination of microstructural properties. *Mater. Sci. Forum* 443–444, 123–126.
- Rodríguez-Navarro, A.B., McCormack, H.M., Fleming, R.H., Alvarez-Lloret, P., Romero-Pastor, J., Dominguez-Gasca, N., Prozorov, T., Dunn, I.C., 2018. Influence of physical activity on tibial bone material properties in laying hens. *J. Struct. Biol.* 201, 36–45.
- Rogers, K.D., Daniels, P., 2002. An X-ray diffraction study of the effects of heat treatment on bone mineral microstructure. *Biomaterials* 23, 2577–2585.
- Schmahl, W.W., Kocsis, B., Toncalo, A., Wycisk, D., Grupe, G., 2017. The crystalline state of archaeological bone material. In: *Across the Alps in Prehistory*. Springer International Publishing.
- Shemesh, A., 1990. Crystallinity and diagenesis of sedimentary apatites. *Geochim. Cosmochim. Acta* 54, 2433–2438.
- Shipman, P., Foster, G., Schoeninger, M., 1984. Burnt bones and teeth: an experimental study of color, morphology, crystal structure and shrinkage. *J. Archaeol. Sci.* 11, 307–325.
- Sillen, A., Hoering, T., 1993. Chemical characterization of burnt bones from Swartkrans. In: Brain, C.K. (Ed.), *Swartkrans: A Cave's Chronicle of Early Man*. Transvaal Museum

- Monograph Vol. 8. Transvaal Museum, Pretoria, pp. 243–249.
- Smith Jr., D.K., Leider, H.R., 1968. Low-temperature thermal expansion of LiH, MgO and CaO. *J. Appl. Crystallogr.* 1, 246–249.
- Snoeck, C., Lee-Thorp, J.A., Schulting, R.J., 2014. From bone to ash: compositional and structural changes in burned modern and archaeological bone. *Palaeogeogr. Palaeoclimatol. Palaeoecol.* 416, 55–68.
- Stiner, M.C., Kuhn, S.L., Weiner, S., Bar-Yosef, O., 1995. Differential burning, re-crystallization, and fragmentation of archaeological bone. *J. Archeol. Sci.* 22, 223–237.
- Thompson, T.J.U., 2005. Heat-induced dimensional changes in bone and their consequences for forensic anthropology. *J. Forensic Sci.* 50, 1008–1015.
- Thompson, T.J.U., Chudek, J.A., 2007. A novel approach to the visualisation of heat-induced structural change in bone. *Sci. Justice* 47, 99–104.
- Thompson, P., Cox, D.E., Hastings, J.B., 1987. Rietveld refinement of Debye–Scherrer synchrotron X-ray data from  $\text{Al}_2\text{O}_3$ . *J. Appl. Crystallogr.* 20, 79–83.
- Thompson, T.J.U., Gauthier, M., Islam, M., 2009. The application of a new method of Fourier Transform Infrared Spectroscopy to the analysis of burned bone. *J. Archeol. Sci.* 36, 910–914.
- Thompson, T.J.U., Islam, M., Piduru, K., Marcel, A., 2011. An investigation into the internal and external variables acting on crystallinity index using Fourier Transform Infrared Spectroscopy on unaltered and burned bone. *Palaeogeogr. Palaeoclimatol. Palaeoecol.* 299, 168–174.
- Thompson, T.J.U., Szigeti, J., Gowland, R.L., Witcher, R.E., 2016. Death on the frontier: military cremation practices in the north of Roman Britain. *J. Archaeol. Sci. Rep.* 10, 828–836.
- Tonegawa, T., Ikoma, T., Yoshioka, T., Hanagata, N., Tanaka, J., 2010. Crystal structure refinement of A-type carbonate apatite by X-ray powder diffraction. *J. Mater. Sci.* 45, 2419–2426.
- Vandecandelaere, N., Rey, C., Drouet, C., 2012. Biomimetic apatite-based biomaterials: on the critical impact of synthesis and post-synthesis parameters. *J. Mater. Sci. Mater. Med.* 23, 2593–2606.
- Von Endt, D.W., Ortner, D.J., 1984. Experimental effects of bone size and temperature on bone diagenesis. *J. Archaeol. Sci.* 11, 247–253.
- Wahl, J., 1982. Leichenbranduntersuchungen. Ein Überblick über die Bearbeitungs- und Aussagemöglichkeiten von Brandgräbern. *Prähistorische Zeitschrift* 57, 1–125.
- Walker, P.L., Miller, K.W.P., Richman, R., 2008. Time, temperature, and oxygen availability: an experimental study of the effects of environmental conditions on the color and organic content of cremated bone. In: *The Analysis of Burned Human Remains*. Academic Press, San Diego, pp. 129–135.
- Wargadalam, V.J., Löffler, G., Winter, F., Hofbauer, H., 2000. Homogeneous formation of NO and  $\text{N}_2\text{O}$  from the oxidation of HCN and  $\text{NH}_3$  at 600–1000 °C. *Combust Flame* 120, 465–478.
- Weiner, S., Bar-Yosef, O., 1990. State of preservation of bones from prehistoric sites in the near east: a survey. *J. Archaeol. Sci.* 17, 187–196.
- Weiner, S., Goldberg, P., Bar-Yosef, O., 1993. Bone preservation in Kebara cave, Israel using on-site Fourier transform infrared spectrometry. *J. Archaeol. Sci.* 20, 613–627.
- Weiner, S., Traub, W., Wagner, H.D., 1999. Lamellar bone: structure-function relations. *J. Struct. Biol.* 126, 241–255.
- Wilson, R.M., Elliot, J.C., Dowker, S.E.P., 1999. Rietveld refinement of the crystallographic structure of human dental enamel apatites. *Am. Mineral.* 84, 1406–1414.
- Wilson, R.M., Elliott, J.C., Dowker, S.E.P., Smith, R.I., 2004. Rietveld structure refinement of precipitated carbonate apatite using neutron diffraction data. *Biomaterials* 25, 2205–2213.
- Wopenka, B., Pasteris, J.D., 2005. A mineralogical perspective on the apatite in bone. *Mater. Sci. Eng. C* 25, 131–143.
- Yi, H., Balan, E., Gervais, C., Segalen, L., Fayon, F., Roche, D., Person, A., Morin, G., Guillaumet, M., Blanchard, M., Lazzari, M., Babonneau, F., 2013. A carbonate-fluoride defect model for carbonate-rich fluorapatite. *Am. Mineral.* 98, 1066–1069.